Generation and characterization of monoclonal antibodies against a cyclic variant of Hepatitis C Virus E2 epitope 412-422.

Annamaria Sandomenico[a], Antonio Leonardi[b], Rita Berisio[a], Luca Sanguigno[b*], Giuseppina Focà[a,c**], Annalia Focà[a,c**], Alessia Ruggiero[a], Nunzianna Doti[a], Livio Muscariello[d], Daniela Barone[a,e], Claudio Farina[d], Ania Owsianka[f], Luigi Vitagliano[a#], Arvind H. Patel[f#], Menotti Ruvo[a#]

[a]*Institute of Biostructures and Bioimaging, CNR and CIRPeB, University of Naples Federico II, Napoli, Italy;* [b]*Dept. of Molecular Medicine and Medical Biotechnology, University of Naples Federico II, Napoli, Italy;* [c]*Dept. of Pharmacy, University of Naples Federico II, Napoli, Italy;* [d]*Kedrion SpA, Lucca, Italy;* [e]*Second University of Naples,* [f]*Medical Research Council - University of Glasgow Centre for Virus Research, Glasgow, UK.*

Running Head: *MAbs against cyclic E2 Epitope 412-422*

[#]Corresponding authors.

Address correspondence to: Menotti Ruvo (menotti.ruvo@unina.it) and Arvind Patel (arvind.patel@glasgow.ac.uk)

Menotti Ruvo and Luigi Vitagliano are co-senior authors of the papers.

*Present affiliation: *Bioker Multimedica, Napoli, Italy*

**Present affiliation*: Institute of Biostructures and Bioimaging, CNR, Napoli, Italy*

Abstract: 234 words

Text: 9247 words

Abstract (max 250 words, currently 234)

Hepatitis C virus (HCV) E2 envelope glycoprotein is crucial for virus entry into hepatocytes. A conserved region of E2 encompassing amino acids 412-423 ~~(epitope I)~~ and containing Trp420, a residue critical for virus entry, is recognized by several broadly neutralizing antibodies. Peptides embodying this epitope ~~I~~ sequence adopt a β-hairpin conformation when bound to neutralizing monoclonal antibodies (MAbs) AP33 and HCV-1. We therefore generated new mouse MAbs that were able to bind to a cyclic peptide containing E2 residues 412-422 (C-Epitope I) but not to the linear counterpart. These MAbs bound to purified E2 with affinities of about 50 nM, but they were unable to neutralize virus infection. Structural analysis of the complex between C-Epitope I and one of our MAbs (C2) show that the Trp420 side chain is largely buried in the combining site and that the Asn417 side chain, which is glycosylated in E2 and solvent-exposed in other complexes, is slightly buried upon C2 binding. Also, the orientation of the cyclic peptide in the antibody combining site is rotated by 180° compared to other complexes. All these structural features, however, do not explain the lack of neutralization activity. This is instead ascribed to the high selectivity of the new MAbs for the cyclic epitope and to their inability to interact with the epitope in more flexible and extended conformations, which recent data suggest play a role in the mechanisms of neutralization escape.

Importance (max 150 words, currently 149)

Hepatitis C virus (HCV) remains a major health care burden affecting almost 3% of the global population. The conserved epitope ~~I~~ comprising residues 412-423 of the viral E2 glycoprotein, is a valid vaccine candidate because antibodies recognizing this region exhibit potent neutralizing activity. This epitope adopts a β-hairpin conformation when bound to neutralizing MAbs. We explored the potential of cyclic peptides mimicking this structure to elicit anti-HCV antibodies. MAbs that specifically recognize a cyclic variant of the epitope bind to soluble E2 with lower affinity than other blocking antibodies and don't

neutralize virus. The structure of the complex between one such MAb and the cyclic epitope, together with new structural data showing the linear peptide bound to neutralizing MAbs in extended conformations, suggests that the epitope displays a conformational flexibility that contributes to neutralization escape. Such features can be of major importance for the design of epitope-based anti-HCV vaccines.

Introduction

Hepatitis C virus (HCV), a positive-strand RNA virus belonging to the Flaviviridae family, infects nearly 3% of the world population (1). In approximately 70-80% of patients HCV establishes a chronic infection in the liver that can lead to cirrhosis, liver failure, and hepatocellular carcinoma (2). HCV exhibits a high degree of genetic variability and is classified into seven major genotypes, each containing a large number of related subtypes (3, 4). This diversity and the high intra-host variability (quasispecies) contribute to virus persistence in the infected hosts. The recently developed new therapies have profoundly improved cure rates. However, higher costs associated with these new medications are expected to limit their wider utilization (5-7). As yet there is no vaccine available against the virus.

HCV entry into target cells is believed to be mediated by a multistep process involving the interplay of the viral envelope glycoproteins E1 and E2 and several host cell factors such as heparan sulfate, tetraspanin CD81, scavenger receptor class-B type I (SR-BI), and the tight junction (TJ) proteins claudin-1 (CLDN1) and occludin (8). E1 and E2 are transmembrane proteins with extensive N-linked glycosylation (4 and 11 N-linked glycosylation sites, respectively) consisting of a large N-terminal ectodomain and a C-terminal hydrophobic anchor (9). The ectodomain of E2 protein contains three highly variable regions. The hypervariable region 1 (HVR1, residues 384-411), located at the N terminus of E2, plays an important role in HCV entry, antibody binding and disease outcome (10). It is now well

established that E2 binds CD81 and SR-B1 and that these interactions are a prerequisite for virus entry (10-13). However, the precise role of E1-E2 envelope protein complex in HCV entry is still unclear.

The viral glycoprotein E2 is the major target for neutralizing antibodies. The majority of broadly neutralizing anti-E2 antibodies isolated to date target epitopes spanning the reported CD81 binding sites of E2. Importantly, mouse MAb AP33 (14), rat MAb 3/11 (15), human MAbs HCV1 (16), HC33 (17) and Hu5B3.v3 (18) block the interaction of E2 to CD81 by binding to linear epitopes located within the highly conserved E2 site encompassing residues 412–423, referred to as Antigenic Site 412 (AS412) (19), or epitope I (20). Other Mabs recognize discontinuous E2 epitopes overlapping with the CD81 binding site on E2 and involving residues 395–424, 425–447, and/or 523–540 (21-22). Residues 412-423 have been proposed as a potential target for HCV vaccine design (18, 25-28).

Although two independent crystal structures of HCV E2 have been recently reported (29, 30), they do not provide any structural data for the region 412-423. Indeed, the construct used by Khan and co-workers (29) spanned E2 residues 456 to 656 whereas in the structure described by Kong and co-workers (30) the N-terminal portion encompassing the 412-423 region is disordered in the crystal. Interestingly, a peptide representing this antigenic site when complexed with neutralizing MAbs AP33, Hu5B3.v3 or HCV1 adopts a β-hairpin conformation, in which Leu413, Gln415, Gly418 and Trp420 are key residues directly involved in the hydrophobic binding surface (18, 26-28). Since the hairpin-like structure of the antibody-bound peptides suggests that region 412-423 adopts a similar conformation in the context of the protein, we designed and prepared a cyclic variant of the epitope to help the fragment to assume a structure alike. The cyclic peptide was used to immunize mice with a view to isolating novel anti-E2 MAbs. By a subtractive screening approach we selected a sub-set of MAbs recognizing only the cyclic antigen to explore the possibility of generating AP33-like antibodies with improved binding affinity and neutralization potency. We reasoned that such an approach might generate antibodies with the potential to more efficiently capture and lock the epitope in a conformation close to that it putatively adopts in the

context of the protein in complex with neutralizing antibodies. However, these MAbs unexpectedly failed to neutralize virus infection. X-ray studies of the complex of one of these MAbs with the cyclic peptide, together with antigen-antibody reactivity data, provide possible explanations for the lack of neutralization activity and offer novel insights for designing vaccine candidates targeting the 412-423 antigenic site.

Materials and Methods

Reagents

TRIzol was purchased from Invitrogen (Carlsbad, CA, USA). The protein G and A columns, and Reagents for Surface Plasmon Resonance were purchased from GE Healthcare. Freund's complete and incomplete adjuvant, and all media including Dulbecco's modified Eagle's medium (DMEM), OPTI-MEM and serum were purchased from GIBCO (Life Technologies, Italia**)** and Sigma-Aldrich (Milan, Italy)**.** The RPMI 1640 medium, containing 10% Fetal Bovine Serum (FBS) and 1% Penicillin, Streptomycin and Glutamine (PSG) was used for maintaining myeloma cells. The RPMI-GM medium contained RPMI 1640 with added 1% non-essential amino acids. For the fusion of splenocytes and myeloma cells we used an RPMI 1640 medium supplemented with 15% FBS, 2% HAT (Hypoxanthine-Aminopterin-Thymidine), 1% PSG and 10% HES (Hybridoma Enhancing Supplement). The same medium, lacking HES, was used for hybridoma clone selection. Reagents for peptide synthesis were from Novabiochem (Laufelfingen, CH), Inbios (Napoli, Italy) and GL Biochem (Shanghai, PRC). Solvents for peptide synthesis and purification were from Romil (Dublin, Ireland). Other reagents were from Sigma-Aldrich (Milano, Italy). KLH (Keyhole Limpet Hemocyanin) was from Pierce-ThermoFisher (Milano, Italy). The broadly neutralizing mouse MAb AP33 has been described previously (14, 31). It was generated following immunization of Balb C mice with a mammalian cell-expressed recombinant secretory form of the HCV genotype 1a strain Gla E1E2 lacking their respective transmembrane domains (32). Soluble E2 (hereafter sE2), amino acids 384-661 (Genbank Accession No. AF009606, genotype 1a

122 strain H77) was expressed by infecting High Five insect cells with a recombinant baculovirus, and the
123 protein secreted into the medium was purified by Ni-NTA chromatography.
124
125 **Peptide design, synthesis and purification**
126 Peptides were prepared under standard conditions of Fmoc solid phase synthesis (33). A cyclic peptide
127 corresponding to region 412-422 of E2 (sequence QLINTNGSWHI) was designed to facilitate the linear
128 epitope to adopt a hairpin-like conformation. The structures of the complexes of the linear peptides
129 corresponding to epitope 412-422 with MAbs AP33, Hu5B3.v3 and HCV1 (26-28) were used as a guide
130 in the design. The peptide was generated by replacing Ile411 and Asn423 of E2 with two cysteines, which
131 were then oxidized to form a disulphide bridge (Figure 1A). Two lysine residues were added at the N-
132 terminus to allow conjugation to KLH and to BSA via glutaraldehyde (amine-to-amine crosslinking).
133 This peptide was here named C-Epitope I. The linear variant (hereafter L-Epitope I) used in the
134 experiments as a control was obtained by alkylation of the cysteine thiols. Alanine-mutated variants of C-
135 Epitope I were designed and prepared under the same conditions to investigate the contribution of specific
136 residues to recognition by antibodies. To overcome the structural similarity of alanine with some of the
137 native residues, we replaced the dyad Gly417-Ser418 with glutamic acids in peptide mutant III. After
138 synthesis and purification, peptides were cyclized as reported elsewhere (34). To suppress cysteine
139 reactivity, the linear peptide was methylated with methyl iodide as reported previously (35). Methylation
140 was chosen as the modification introducing the minimum structural change within the molecule.
141
142 **Circular dichroism**
143 The purified cyclic peptide was characterized by Circular Dichroism (CD) using a JASCO J-710
144 spectropolarimeter (JASCO Corp.), equipped with a Peltier temperature control system and a 110-QS
145 quartz cuvette with 1.0-cm path length. Spectra were collected on peptide solutions at 0.1 mM in 10 mM

phosphate buffer, pH 7.0, using the following settings: wavelength range, 190-280 nm; scanning speed, 20 nm/min; data pitch, 0.2 nm; band width, 1 nm; response time, 4 s. Recorded spectra were signal-averaged from at least five independent readings and smoothed.

Immunogen preparation

One mg of C-Epitope I was conjugated with 3.0 mg of carrier proteins (KLH or BSA) in 2.0 ml of 20 mM phosphate buffer pH 7.0 containing 0.2% v/v glutaraldehyde by stirring the mixture for 3 h. One ml of 1 M glycine in water was added to block the reaction, then solutions were extensively dialyzed against PBS pH 7.4 before being lyophilized. The amount of peptide-protein conjugate was determined using a BIORAD kit (BioRad, Milano). The same procedure was used to prepare glutaraldehyde self-conjugated BSA (BSA_2). BSA_2 was used in the ELISA assay as control to exclude clones producing antibodies potentially recognizing the amine cross-linked glutaraldehyde (36).

Immunization of mice and generation and purification of MAbs

BALB/c mice were housed and handled according to the institutional guidelines (Project identification code 2013/0038120, approved by the Ethical Animal Care and Use Committee, University of Naples "Federico II". Date of approval April 24th 2013). Four 5-week old Balb/c mice (Jackson Lab) were immunized with 100 µg of KLH-conjugated peptide emulsified with Complete Freund's adjuvant. Four independent injections were carried out subcutaneously with 25 µl immunogen. Before immunization, 250 µl blood samples were taken from each mouse from the caudal vein and used as the pre-immune control (T_0 samples). Mice were boosted with the same amount of immunogen in incomplete Freund's adjuvant at day 30 after the first immunization. Blood samples were taken from the caudal vein (250 µL) before every subsequent boosting and tested by ELISA to monitor antibody titer. A final antigen boost

169 was administered intravenously in mice showing the highest antibody titer 20 days before being sacrificed
170 and splenectomised as described below.
171 Cells harvested from spleens of sacrificed animals were fused with myeloma SP2/0 (ATCC) cells at a
172 ratio of 5:1 in RPMI-GM containing polyethylene glycol (PEG) 1300-1600 (Hybri-Max, Sigma-Aldrich,
173 Milano) and 7.5% DMSO (Sigma-Aldrich, Milano) as described (37). The fused hybridoma cells were re-
174 suspended in 30 ml of selection medium consisting of RPMI–GM medium containing PEG 1300-1600,
175 10% FBS, 100 U/ml penicillin, 100 µg/ml streptomycin, 100 µM hypoxanthine, 16 µM thymidine and
176 400 nM aminopterin (RPMI-HAT Sigma-Aldrich, Milano). The cell suspension was dispensed into 96-
177 well plates and incubated at 37 °C in a 5% CO_2 atmosphere with periodic replenishment with fresh
178 selection medium. After 12 to 14 days, cell medium was screened by ELISA for binding to C-Epitope I
179 and to its linear analogue. Hybridomas secreting antibodies with strong reactivity with C-Epitope I (but
180 not L-Epitope I) were re-cloned twice by limiting dilution, and their reactivity re-confirmed by ELISA.
181 Sub-cloned hybridoma cells were cultured in OPTI-MEM medium containing 10% FBS, adapted
182 gradually to serum-free cell medium, and then transferred to bioreactors (INTEGRA Biosciences AG,
183 CH-7000 Chur, Switzerland) for large-scale antibody production. Antibodies were purified to
184 homogeneity by protein G affinity chromatography followed by gel filtration. Antibodies were
185 characterized by SDS-PAGE, analytical size-exclusion chromatography and western blotting.
186 Immunoreactivity of purified antibodies with antigen was determined by ELISA, as described below.
187
188 **Fab fragment generation and purification**
189 Briefly, Fab fragments were prepared by papain digestion of purified IgGs. The reaction, monitored by
190 SDS-PAGE, was optimized in 20 mM sodium phosphate and 10 mM EDTA pH 7.0 buffer using papain
191 1:100 w/w ratio (Sigma-Aldrich, Milano) for 3 h at 37 °C. The Fc portion was removed using a HiTrap
192 Protein G column (GE Healthcare, Milano), then the Fab fragment was further purified by gel filtration

on a Sephadex 75 column (GE Healthcare, Milano) in PBS or 25 mM Tris-HCl, 100 mM NaCl pH 7.5. Concentration and purity of antibodies and Fab fragments were estimated by absorbance at 280 nm using NanoDrop 2000, SDS-PAGE and size exclusion high performance liquid chromatography.

ELISA assays

Titrations of antibody in mouse sera and screening of hybridoma supernatants were performed by Enzyme-Linked Immunosorbent Assays (ELISA). Antibody titrations in mouse sera and screening of hybridoma supernatants were performed by Enzyme-Linked Immunosorbent Assays (ELISA) as described elsewhere (38). Hybridomas were screened for their ability to secrete MAbs specific for the cyclic antigen. For this purpose, supernatants were tested by coating plates with both BSA-conjugated C-Epitope I and BSA-conjugated L-Epitope I. Also BSA_2 was used as control to exclude clones producing antibodies recognizing the BSA-linked glutaraldehyde. Positive clones were stabilized by 3 sequential rounds of limiting dilution passages in 96-well plates. Following incubation for 2 weeks at 37 °C under 5% CO_2, supernatants from each well were again tested for the presence of antibodies against the peptide antigen. Hybridomas secreting the highest antibody titer were further subjected to 3 rounds of limiting dilution cloning. Finally, antibodies secreted by selected hybridomas were purified and tested by ELISA for reactivity to the free C-Epitope I and its linear variant. Briefly, ELISA (Nunc, Maxisorp) plate wells were coated with the appropriate peptide at 0.5 µg/ml in PBS by incubating overnight at 4 °C. The wells were blocked with BSA and then washed with PBS-T as described above. Antigen-coated wells were incubated with 0.5 µg/ml of appropriate antibodies at 37 °C for 60 min, washed as above and then further incubated with HRP-conjugated anti-mouse IgG (1:1000, Biorad) at 37 °C for 60 min. After washing, the bound antibody was detected by adding peroxidase substrate solution (prepared by dissolving o-phenylenediamine dihydrochloride at 0.4 mg/ml in 0.1 M citric acid and 0.2 M Na_2HPO_4 buffer (pH 4.8) and adding 0.2 µl/ml of 30% H_2O_2). Following incubation at room temperature in the dark, the reaction

was stopped with a 2.5 M H_2SO_4 solution, and the optical density at 492 nm was determined using a microplate reader (BioTek, Winooski, VT, USA). Specificity was assessed using an unrelated monoclonal antibody (Trastuzumab, Genentech) indicated as negative control (NC) and MAb AP33 as a positive-control, at the same concentrations.

An ELISA to detect MAb binding to mammalian cell-expressed sE2, full-length (FL) E2 and E1E2 glycoprotein was performed essentially as described previously (14, 39). Briefly, HEK293T cells were co-transfected with appropriate sequence-containing plasmids, and the expressed glycoproteins present in larified lysates of these cells were captured on to GNA (Galanthus Nivalis Agglutinin)-coated Immulon II enzyme immunoassay (EIA) plates (Thermolab systems). Anti-E2 MAbs were added, and bound glycoproteins were detected with an anti-mouse immunoglobulin G-horseradish peroxidase (Sigma, United Kingdom) and TMB (3,3,5,5-tetramethylbenzidine; Sigma, United Kingdom) substrate. Absorbance values were determined at 450 nm. Screening assays of clones were performed at least twice in quadruplicates. Data are reported as average of results from all experiments and replicates ± standard deviation (± SD). Binding assays of MAbs to peptides and recombinant proteins were performed at least twice. Data are reported as average of results from all experiments and replicates ± SD.

Sequencing of antibody variable regions and isotype determination.

To clone the Ig heavy and light chain variable region genes encoding a subset of the anti-E2 MAbs, total RNA from hybridoma cells was used first to generate cDNA libraries by reverse transcription reactions with a SuperScript III first-strand kit (Invitrogen) using random hexamers. The IgG Fab fragments corresponding to the antigen-binding variable regions were then amplified by polymerase chain reaction (PCR) using a set of heavy-chain and light-chain primers specific for mouse Ig. The nucleotide sequences of PCR products were determined and their amino acid sequences deduced using the program "Translate"

from ExPASy proteomic server. The isotypes of the MAbs were determined using a Monoclonal Antibody Isotyping Kit [IsoStrip, Pierce, Rockford, IL USA] according to the manufacturer's instructions.

SPR analysis

All SPR analyses were performed on a Biacore 3000 instrument from GE Healthcare, using CM5 sensor chips and certified HBS buffer (20 mM HEPES, 0.15 M NaCl, pH 7.2, P20, 0.005%), at 25 °C. Immobilization was carried out following the canonical amine coupling chemistry using the surface immobilization wizard procedure operating at 5 µl/min. Channels were activated with EDC/NHS mixture for 7 min; then the ligand, appropriately diluted in the pre-selected sodium acetate buffer, was coupled until a typical 500-600 RU level was achieved. Remaining active ester groups were blocked with 1 M ethanolamine HCl, pH 8.5. SPR binding measurements to L-Epitope, C-Epitope I and alanine-mutated variants, were carried out by immobilizing each antibody or Fabs on CM5 sensor chips. Antibody immobilization, including AP33, was efficiently performed at 5.0 µg/ml in sodium acetate 10 mM pH 4.5, achieving immobilization levels of around 500-600 RU in every case. The same procedure was applied to prepare a sE2-functionalized sensor chip. An IgG1 isotype-matched antibody was used as negative control at a concentration of 5.0 µM. For epitope mapping, the Fab fragment of the C2 antibody was directly immobilized onto a CM5 sensor chip at 5.0 µg/ml in sodium acetate 10 mM pH 4.5 (immobilization level of around 500-600 RU). On every sensor chip, an underivatized surface was prepared and used as a blank control. All analyses were carried out at a flow rate of 20 µl/min, injecting a constant volume of 60 µl of protein or peptide solutions appropriately diluted in the HBS running buffer. For every analysis, experimental sensorgrams were aligned, blank signal was subtracted and overlapped. All mathematical manipulations and fitting were performed using the BiaEvaluation software, vers. 4.1 (GE Healthcare). All experimental data gave optimal fittings when processed assuming a 1:1 Langmuir binding interaction.

264

265 **HCVcc neutralization assays**

266 Cell culture infectious HCV (HCVcc) was produced by electroporation of human hepatoma cell Huh7
267 with viral genomic RNA that was generated by in vitro transcription using the plasmid pUC-JFH1 or
268 pUC-JFH1-N417T as template as described (40, 41). Virus neutralization assays were performed using
269 Huh7-J20 reporter cells, and virus infectivity levels were determined by SEAP reporter assay, as
270 described previously (42). Briefly, Huh7-J20 cells were plated out at a density of 5 x 10^3 per well in a 96-
271 well plate. Virus was pre-incubated at 37 °C for 1 h with the test antibody prior to infecting cells at m.o.i
272 of 0.1. At 3 h post-infection, the inoculum was replaced with fresh DMEM. At 72 h post-infection SEAP
273 reporter activity (which correlates directly with virus infectivity levels) in the medium of infected cells
274 was determined as described previously (42).

275

276 **Crystallization and diffraction data collection**

277 Crystallization trials on the Fab C2-peptide complex were set up at 293 K using the hanging-drop vapour-
278 diffusion method. The peptide and the Fab were previously mixed with a molar ratio of 4:1. Preliminary
279 screenings of the crystallization conditions were carried out using commercially available sparse-matrix
280 kits (Crystal Screen kits I/II and Index by Hampton Research) (43). These screenings yielded micro-
281 crystals that were optimized by fine-tuning protein and precipitant concentrations. Crystals suitable for
282 crystallographic investigations were obtained using a Fab concentration of ~ 5.0 mg/ml and 0.2 M
283 Ammonium sulphate and 25% (w/v) PEG 3,350 in a buffer containing 0.1 M Bis-Tris pH 5.5.
284 Diffraction data were collected in-house at 100K using a Rigaku Micromax 007 HF generator producing
285 Cu Kα radiation and equipped with a Saturn944 CCD detector. Data were collected at 100 K by adding a
286 solution of 20% (v/v) ethylene glycol as a cryoprotectant to the precipitating solution. The data set was
287 scaled and merged using HKL2000 program package (44). Although two angles of the unit cell were

numerically close to 90°, the crystals of the complex are triclinic. Indeed, all attempts to process the data with higher symmetry yielded very high R_{merge} values. The analysis of the V_m value of this crystal suggests the presence of two molecules in the asymmetric unit.

Crystallographic refinement

The structure of the complex was solved by molecular replacement using Phaser (45). Starting models for the light and the heavy chains were selected by looking for PDB structures with the highest sequence identities with the chains of our Fab. Using this approach, the starting models for the heavy and light chains were extracted from the PDB structures 2VL5 (identity 82%) and 3DGG (identity 94%), respectively. Taking into account the variability of the relative orientation of the constant and variable regions, both heavy and the light chains were fragmented by considering the individual Fab domains. Therefore, since the asymmetric unit contains two independent molecules, an ensemble of eight individual fragments constituted the starting structures in the molecular replacement search. The application of this procedure provided a straightforward solution. This model was used for automatic rebuilding carried out using Arp-Warp (46). Crystallographic refinement was carried out against 95% of the measured data using the ccp4i program suite. The remaining 5% of the observed data, which was randomly selected, was used in R free calculations to monitor the progress of refinement. Non crystallographic restraints were applied in REFMAC (47) with medium restraints for main-chain atoms and loose restraints for side-chain atoms. Manual modelling was performed using Coot (48). Water molecules were incorporated into the structure in several rounds of successive refinements. The coordinates of the model and the experimental structure factors of the complex are being deposited in the PDB (entry code 5EOC).

Molecular dynamic studies

In order to gain insights into the intrinsic conformational properties of the cyclic peptide, a molecular dynamics (MD) simulation was conducted using the structure of the peptide detected in the complex with Fab C2 as starting model. The Molecular dynamics simulation was performed using GROMACS software package 4.5.5 (49), the AMBER99sb force field and TIP4P as water model. The peptide was immersed in a cubic box of 4.50x4.50x4.50 nm^3 containing 2933 water molecules. The simulation was run with periodic boundary conditions. The temperature and pressure of the systems were stabilized at 300 K and 1 atm, respectively. Energies were minimized by fixing the protein atoms and then without restraints. The timescale of the simulation was 250 ns, with a time step of 0.002 ps. The Particle Mesh Ewald (PME) method (grid spacing of 0.12 nm) was used to calculate the electrostatic interactions. A cutoff of 10 Å was applied to treat Lennard-Jones interactions. Bond lengths were constrained by the LINCS procedure. Trajectories were checked to assess the quality of the simulation using GROMACS routines. H-bond interactions were identified based on cutoffs for the angle hydrogen-donor–acceptor (~30°) and the distance donor–acceptor (~3.5 Å) by using GROMACS utilities (49).

RESULTS

Production and selection of MAbs against C-Epitope I

Hybridoma cell supernatants were directly screened against both C-Epitope I and its linear (L) variant conjugated to BSA. Hybridomas secreting antibodies able to specifically recognize the cyclic peptide were selected for further studies. This screening strategy led to the selection of seven different hybridoma clones renamed C1 to C7 (Figure 1B). BSA_2 was used in the subsequent tests to exclude antibodies binding to glutaraldehyde-cross-linked BSA. These data were confirmed in ELISA binding assays where the free, unconjugated peptides were coated on the plate surface. The selected MAbs bound to C-Epitope I in a dose-dependent fashion (Figure 1C), but not to the L-Epitope or the BSA_2 control (Figure 1C). As

expected, an unrelated IgG1 isotype-matched MAb, used as a negative control (NC), did not recognise either peptide (Figure 1B). MAb AP33, used as positive control, bound to both the cyclic and linear peptides (Figure 1D). A more detailed characterization of peptide binding to all antibodies was performed by SPR (see below). All selected MAbs were of the IgG_1 isotype with kappa light chains.

Evaluation of binding affinity of MAbs C1 to C7 for C-Epitope I

Binding analyses were performed by SPR, with the purified antibodies immobilized on distinct channels of CM5 sensor chips. SPR dose-response binding assays confirmed that only the cyclized peptide bound the MAbs with very high affinity (Figure 2A-G and Table 1) while no or very poor interactions were observed with the linear variant (tested at the highest concentration of 10 µM; Figure 2H). The cyclic peptide bound all the immobilized MAbs with similar association kinetics. Dissociations were instead much slower for MAbs C6 and C7, which exhibited K_D values of about 0.9 nM and 0.7 nM, respectively (Table 1). The other MAbs showed K_Ds ranging from 10 nM to 50 nM. MAb AP33, raised against a recombinant soluble form of E1E2 (32), had a 150-fold higher affinity to the linear peptide than to the cyclic one (K_D = 0.5 nM versus K_D = 71 nM) (Figure 2I-L and Table 1).

Binding of MAbs to recombinant sE2 protein

We next evaluated the ability of antibodies to recognize recombinant soluble E2 (sE2) (the relative purity of this protein is shown in Figure 3). For this purpose, dose-dependent binding assays were carried out on a sE2-functionalized CM5 sensorchip. Binding of AP33 was observed at concentrations ranging from 0.125 nM to 1 nM while the interaction with anti-C-Epitope I antibodies was observed at MAbs concentrations ranging from 100 nM to 1 µM (Figure 3A-F). In line with these observations, SPR kinetics and affinity parameters, summarized in Table 2, show that AP33 binds sE2 with a considerably higher affinity (K_D = 0.142 nM) than anti-C-Epitope I MAbs which, with the exception of C7, exhibit K_D values

around 50 nM. As expected, no binding to sE2 was detected using a isotype-matched unrelated IgG1 even at concentrations as high as 5 μM (Figure 3G).

Collectively, SPR data indicate that anti-C-Epitope I MAbs are able to recognize the recombinant soluble E2 protein, although their affinities are significantly lower than that to the C-Epitope I peptide, and than that exhibited by AP33. It is worth noting that AP33 binds more efficiently to sE2 than to either the C-Epitope I peptide (K_D of about 71 nM, Table 1) or the linear L-Epitope I peptide (K_D about 0.5 nM, Table 1). We wished to test whether MAbs could bind not only to sE2 but also to the full-length (FL) E2 protein and the E1E2 heterodimer. Transient transfection of HEK cells was used to produce sE2, FL E2 and E1E2. Proteins from cell extracts were captured onto GNA-coated ELISA plates. Addition of anti-C-Epitope I MAbs C2, C3, C4, C5 and C7 at 10 μg/ml gave a weak binding signal with C2 only, while no binding was observed with the other MAbs (Figure 4). In contrast, MAb AP33 at 0.02 μg/ml gave a strong signal with all forms of the glycoprotein (Figure 4).

We next tested whether MAbs were capable of neutralization of HCVpp and HCVcc. We found that, unlike MAb AP33, all anti-C-Epitope I MAbs (used at 50 and 100 μg/mL, that is 335 and 670 nM, respectively) failed to neutralize HCVpp bearing E1E2 derived from HCV genotype 1a strain H77 (data not shown). Similarly, these MAbs were also unable to neutralize infection of Huh-7 cells with the genotype 2a strain JFH-1 HCVcc (data not shown; see for example also Figure 5). Collectively, these data are in agreement with the lack of sE2 binding exhibited by anti-cyclic peptide MAbs, although in consideration of the concentration used in the neutralization tests and the KDs measured by SPR, they do not fully explain the complete absence of activity. Biacore binding measurements between sE2 and the Fabs of both C2 and AP33 showed that both MAbs displayed an average 5-fold affinity reduction when only one antibody arm was used (see Table 2), a result suggestive of an avidity effect exhibited by both antibodies.

Crystal structure of Fab C2 in complex with C-Epitope I

To gain insights into the structural basis of the limited affinity of these MAbs for sE2 and the lack of neutralization activity, we performed crystallographic analyses of Fab complexes with the C-Epitope I peptide. Although we were able to obtain crystals or microcrystals of all the Fabs bound to the C-Epitope-I peptide, only the Fab C2-peptide complex was suitable for crystallography. The structure of this complex was determined to 1.98 Å resolution. The triclinic crystals used for the crystallographic investigations contain two independent copies of the complex. The structures of these two crystal mates are very similar. Indeed, the root mean square deviations computed on the C^{α} atoms is 0.58 Å. Therefore, the structural feature of molecule A (Figure 6A) corresponding to the heavy (H) and light (L) chains was analysed further. The Fab is composed of the canonical four immunoglobulin subunits. The elbow angles for the two Fab molecules in the asymmetric units are 129° and 131°. These values falls in the range observed for Kappa Fab structures (50). The CDR loops of the Fab C2 are also similar to those observed in canonical structures (51). Since the early stages of the refinement of the complex, the inspection of the electron density maps clearly indicated the presence of peptide in a cleft formed by the variable regions of the light and heavy chains. As shown in Figure 6B, the electron density is well defined for all residues of the peptide, including the two cysteine residues that form the disulphide bridge that closes the loop. The peptide adopts a β-hairpin structure that is stabilized by five hydrogen bonds, four involving main chain atoms and one the side chains. Two backbone H-bonds are formed by the nitrogen and the carbonyl of Gln412 with the carbonyl and the nitrogen of Ile422, respectively. A similar pair of bonds is formed by Ile414 and Trp420. The network of intra-peptide H-bonds is completed by the one formed by the side chains of Trp420 (atom $N^{\varepsilon 1}$) and Thr416 (atom $O^{\gamma 1}$). (Figure 6C).

Peptide binding by the Fab C2 relies on hydrophobic interactions and H-bonds established at the antibody combining site (Figure 6D and 6E). Both the heavy and the light chains of C2 contribute to the binding. The surface buried upon peptide binding is 353 $Å^2$ and 195 $Å^2$ for the light and the heavy chains,

408 respectively. The interactions of the light chain with the peptide involve the complementarity-determining
409 regions (CDRs) L1 and L3. In line with other complexes of Fabs with peptides, no interactions are
410 established by CDR L2. On the other hand, all three H-chain CDRs establish interactions with the
411 peptide. The main hydrophobic interactions are established by Tyr36 (CDR L1), Ile 95 (CDR L3), and
412 Trp33 (CDR H1) with the nonpolar residues of the peptide (Trp420 and Ile422). Most of the H-bonding
413 interactions involve charged side chains of the Fab. Indeed, Arg59 (CDR H2) and Asp103 (CDR H3) side
414 chains of the heavy chain bind Asn417 and Trp420 of the peptide, respectively. Moreover, the side chains
415 of Arg96 and Arg100 of CDR L3 bind the carbonyl groups of the main chain of Asn415 and Thr416,
416 respectively. The ensemble of these intermolecular H-bonds is completed by the one formed by the side
417 chain of Ser32 (CDR L1) and the carbonyl group of Ile422. Crystallographic and stereo-chemical
418 statistics of the final models are summarized in Table 3.
419
420 **Molecular dynamic and circular dichroism studies**
421 The intrinsic conformational properties of the cyclic peptide were analyzed by MD. These studies were
422 conducted using the conformation of the peptide observed in the complex with the Fab C2 as starting
423 model. The analysis of the trajectory structure clearly indicates that the peptide undergoes significant
424 conformational transition during the MD simulation. Indeed, as shown in Figure 7A root mean square
425 deviations (RMSD) of trajectory structures *versus* the starting crystallographic model present significant
426 variations. A similar behavior is highlighted by the analysis of the gyration radius of the simulation
427 structures (Figure 7B). The analysis of the gyration radius also indicates that the peptide frequently
428 assumes structures that are more compact compared to the elongated β-hairpin motif observed for the
429 peptide in the complex with the antibody. Interestingly, these compact structures occasionally evolve into
430 β-hairpin states resembling the crystallographic one (at approx. at 140 ns, as shown in Figure 7A). These
431 findings indicate (a) that the cyclic peptide is intrinsically endowed with a significant level of flexibility

and (b) that the conformation detected in the complex with Fab C2 is among those intrinsically accessible to the peptide.

The intrinsic flexibility of the C2 peptide is confirmed by a circular dichroism analysis performed in aqueous buffer (see methods for details). Indeed, as shown in Figure 7C, the CD spectrum of the peptide is suggestive of a very limited content of regular structure.

To gain deeper insights into the structural features of the conformational ensemble of the cyclic peptide, we compared the trajectory structures with the conformation adopted by the linear variant when complexed with other Fabs. Not surprisingly, when trajectory structures are compared to the linear peptide adopting the β-hairpin motifs, as in the complex with AP33, the trends are rather similar to those observed for the cyclic peptide (Figure 7A and 7D). We also searched the simulation ensemble for structures showing the highest similarity with the conformation adopted by the linear variant in complex with AP33. The closest trajectory structures present RMSD values against this variant of 1.1 Å. Interestingly, the RMSD displayed by the conformation adopted by cyclic peptide in the Fab C2 complex against the same peptide is larger (1.76 Å). However, although trajectory structure becomes closer to that of the peptide bound to AP33, none of them perfectly reproduces it. As expected, the deviations of trajectory structures versus the elongated conformations of the peptides in complex with the Fabs of HC33.1 and 3/11 are much larger (data not show). This is an obvious consequence of the restraints imposed by the disulfide bridge that impede to the cyclic peptide to adopt highly extended conformations.

C-Epitope I mapping using Fab C2.

To further investigate which peptide residues were mostly involved in the binding with antibodies, we designed and prepared a panel of alanine-mutated cyclic peptides (Table 4**)**. This study was carried out by SPR dose-response binding assays on a sensor chip functionalized with the purified Fab fragment of C2. All peptides were tested at concentrations ranging between 125 nM and 5 μM. As shown in Table 4, we

found that Fab C2 bound the wild type C-Epitope I peptide with a K_D similar to that exhibited by the whole antibody (30.3 nM versus 32.7 nM, respectively). When we tested the peptides bearing mutations across residues 411-418, we observed that the K_D for peptide mutant II, where the Asn-Thr-Asn amino acids were replaced with alanines, was substantially similar to that of the wild type, that is 14.8 nM for mutant II and 32.7 nM for the unmodified peptide. With mutants I and III, the affinity was greatly reduced (Table 4), whereas with mutant IV, bearing mutations on residues 420-422 (Trp-His-Ile), the binding was abolished. The data overall suggested that triplet Trp420, His421 and Ile422, is crucial for antibody recognition. These results are in keeping with the crystallographic findings and provide quantitative information on the role played by specific residues of C-Epitope I in Fab recognition.

Neutralization by C2 of the HCVcc mutant N417T

Our structural data reveal that the N417 side chain is partially buried upon Fab C2 binding (Figure 6D). Since residue N417 is glycosylated in the native protein, we hypothesized that N417 glycosylation could be an important factor in E2 recognition by MAb C2. To further address this issue, we used a virus neutralization assay to evaluate the ability of MAb C2 to recognize an E2 variant carrying the mutation N417T that abolishes this glycosylation site. In this mutant the glycosylation site is shifted to N415, whose side chain is fully exposed in the structure of the complex between Fab C2 and the cyclic peptide (Figure 6D). This glycan shift has been proposed to render E2 resistant to recognition by anti-Epitope-I MAbs such as AP33 (18). As shown in Figure 5A and 5B, MAb C2 failed to neutralize N417T HCVcc as well as the WT virus, while, as expected, MAb AP33 efficiently neutralized the WT virus, but not the N417T mutant (18). This observation indicates that the inability of MAb C2 to recognize HCVcc is not dependent on the glycosylation status of N417.

480 **DISCUSSION**

481 The elevated costs associated with current antiviral hepatitis C therapies and the high disease prevalence
482 necessitates the urgent development of alternative therapeutic approaches. As for many other viral
483 diseases, a vaccine would be the most obvious and less expensive option. However, the high genetic
484 variability of the virus is a major barrier that has so far prevented the generation of effective anti-HCV
485 vaccines. Several studies have indicated that the HCV surface glycoprotein E2 is a major target for
486 neutralizing antibodies. However, they are generally isolate-specific and do not recognize E2 proteins
487 from other HCV genotypes, thus preventing their use as broad-spectrum neutralizing reagents. The
488 conserved region 412-422 of E2 encompassing Trp420, a key residue for HCV recognition by the human
489 receptor CD81 (9, 11), is recognized by several neutralizing antibodies (13-17). Despite the crucial role
490 this epitope residues play in HCV entry, no information on the conformation(s) this region adopts in the
491 context of the E2 protein is available. Structural studies on complexes of E2 peptide 412-423 with three
492 neutralizing MAbs have shown a tendency of this fragment to adopt a β-hairpin conformation (18, 26-28).
493 In this framework, to gain insights into epitope 412-422 conformational preferences, we generated and
494 characterized a set of MAbs that selectively recognize a conformationally-restrained cyclic variant of this
495 epitope but not its linear counterpart. Binding assays demonstrated that such MAbs were able to bind the
496 soluble E2 protein with K_Ds of about 50 nM. This finding holds an interesting implication. Considering
497 that the MAbs are unable to recognize the linear ~~peptide embodying the sequence of~~ epitope ~~I~~, their
498 ability to bind E2 suggests that the protein context has an impact on the epitope structure, likely shifting
499 its conformation towards bent states. However, the affinity for E2 exhibited by these MAbs is
500 significantly lower than that exhibited by the neutralizing MAb AP33 (approximately 500-fold lower) and
501 this feature largely contributes to the lack of activity of the new antibodies.
502 A crystallographic analysis of the complex between the Fab of the C2 MAb and the cyclic peptide was
503 undertaken to unravel the basis of the reduced affinity of the MAbs for the E2 protein and of the

consequent inability to neutralize either HCVpp or HCVcc. A comparison of the crystal structure of the C-Epitope I/Fab C2 complex with the structure of the linear peptide bound to hu5B3.v3, AP33 or HCV-1 Fab (18, 26-28) shows both analogies and differences. Firstly, in all of these complexes the peptide adopts a β-hairpin conformation stabilized by H-bonds established with main chain atoms. Moreover, these peptide-Fab complexes feature a similar buried surface (~ 250 $Å^2$) with an important contribution to intermolecular interactions provided by the side chain of Trp420 (Figure 6D and 6E) (18, 26-28). These observations indicate that the C2 MAb, despite its inability to neutralize virus infection, shares with hu5B3.v3, AP33 and HCV-1 two important features related to the overall peptide conformation and to the tight binding to the Trp420 side chain. A deeper comparison of these complexes underlines, however, some distinct features in the recognition of the cyclic peptide by C2. Particularly, the binding of C-Epitope I by Fab C2 appears to be rotated by 180° compared to other complexes (Figure 8A-D). This leads to differences in the interacting surfaces between the linear and cyclic variant in the complex with their MAbs (Figure 9). In particular, residues such as Leu413 and Asn415, which interact with AP33 and HCV1, are fully exposed in the C2 complex. On the other hand, the side chain of Asn417, which is glycosylated in E2 and exposed to the solvent in the other complexes, is slightly buried upon C2 binding (Figure 6D). It is worth mentioning that the failure of C2 to neutralize variants such as N417T, that cannot be glycosylated at position 417 (18), suggests that the partial burying of Asn417 does not play a major role in determining the distinctive behaviour of C2. Finally, there is a slight shift in the residues involved in the hydrogen bonding patterns of the hairpin in the peptide-C2 complex compared to the others. The previously reported structures show that the hairpin is stabilized by H-bonds formed by residues 414-421 and 412-423 whereas the conformation of the cyclic peptide bound to C2 is stabilized by H-bonds involving residues 412-422 and 414-420. Predictive analyses, carried out using the PEP-FOLD server (http://bioserv.rpbs.univ-paris-diderot.fr/services/PEP-FOLD/), suggest that the structure observed for the cyclic peptide in the complex is similar to the conformation intrinsically accessible to the

528 linear sequence of epitope 412-422. Indeed, the RMSD values of the cyclic peptide structure versus the
529 two top solutions provided by PEP-FOLD are in the range of 1.9-2.0 Å (52). Together, these observations
530 may in principle explain the reduced affinity of C2 MAb for E2 and suggest that the lack of neutralization
531 may originate from a combination of low antibody affinity and inappropriate epitope approaching.
532 Indeed, despite the analogies with other complexes, the specificities of the C2 complex with the cyclic
533 variant in terms of peptide H-bond patterns and side chain conformations, as well as in terms of the
534 relative orientation of the epitope and MAb, may limit the ability of C2 to recognize E2. This implies that
535 the conformations of the linear peptides observed in the HCV1 and AP33 complexes, represents a reliable
536 model of the structure of the epitope in the context of real E2. In this framework, the absence of
537 significant neutralizing effect of the MAbs generated against the cyclic variant is likely due to the
538 inability of this peptide, supported by our MD analysis, to fully reproduce the epitope conformation of the
539 linear variant observed in the complexes with AP33 and HCV1. However, it should be noted that, while
540 this manuscript was in preparation, two novel complexes of neutralizing Fabs 3/11 and HC33.1 in
541 complex with the linear epitope have been reported (53, 54). Surprisingly, in both these new complexes
542 the bound peptides assume rather extended conformations that are completely unrelated to those observed
543 in the complexes with AP33 and HCV1. These new data strongly suggests that epitope 412-422 is, in the
544 protein context, endowed with a remarkable structural versatility, a property believed to be an additional
545 mechanism of neutralization escape (53, 54). The observation that the epitope conformation recognized
546 by Fabs 3/11 and HC33.1 may differ from that observed in AP33 and HCV1 suggests that the specificities
547 of the conformation of the cyclic peptide recognized by C2 may not be the only factor responsible of the
548 inactivity of this MAb.
549 It is likely that our MAbs, which recognize with high selectivity a conformationally restrained variant of
550 epitope 412-422, are unable to accommodate all of its accessible structural states. In other words, these
551 MAbs are able to bind only a sub-population of the diverse conformational ensemble adopted by epitope

Journal of Virology

552 412-422, a property that reflects the reduced affinity of our MAbs for the E2 protein and their inability to
553 display any significant neutralizing activity. On the other hand, neutralizing MAbs such as AP33, that
554 recognize both cyclic and linear variants of epitope 412-422, have a high affinity for E2 since they are
555 able to capture different conformational states of this E2 region. These considerations should be taken
556 into account in the selection of HCV neutralizing MAbs and for the design of new potential vaccines.
557 In conclusion, our data corroborate the emerging notion that epitope 412-422 is characterized within the
558 protein context by a high conformational versatility which likely contributes to a mechanism of
559 conformation-driven neutralization escape. Since rigid and flexible regions in a protein are typically
560 characterized by conserved and variable sequences, respectively, further studies are needed to clarify why
561 and how E2 epitope 412-422 region combines a structural flexibility with a highly conserved local
562 sequence.
563

564 **Funding information.**

565 This work was supported by funds from FIRB MERIT N° RBNE08NKH7_003 and from PON Ricerca e
566 Competitività 2007-2013 (PON01_01602, PON01_02342, PON04a2_C SMART HEALTH) to MR. The
567 project was partially funded by Rete integrata per le biotecnologie applicate a molecole ad attività
568 farmacologica - FarmaBioNet, and progetto BERSAGLI- Bersagli, sonde e segnali in terapia diagnostica
569 (Bando per la Realizzazione della Rete delle Biotecnologie Campane, Obiettivo Operativo 2.1 POR
570 Campania) 2013-2015. The work in AHP's laboratory was supported by the Medical Research Council,
571 UK.
572

573 **Acknowledgments**

574 A.S. designed and performed binding experiments. A.L. conceived experiments and contributed to
575 antibody generation and to analyze data. R.B. and A.R. performed crystallization studies. L.S. made

Journal of Virology

JVI

Journal of Virology

immunization and hybridoma experiments. G.F., N.D. and A.F. performed binding studies, D.B carried out molecular dynamics simulations. L.M. and C.F. produced monoclonal antibodies. A.O. performed neutralization and binding experiments. L.V., A.H.P. and M.R. conceived the work, designed experiments and analyzed the data. A.S., M.R., L.V., A.O. and A.H.P. wrote the paper.

588 **References**

589 1. **Mohd Hanafiah K, Groeger J, Flaxman AD, Wiersma ST**. 2013 Global epidemiology of
590 hepatitis C virus infection: new estimates of age-specific antibody to HCV seroprevalence.
591 Hepatology. **57**(4): 1333-42.

592 2. **Galossi A, Guarisco R, Bellis L, Puoti C.** 2007. Extrahepatic manifestations of chronic HCV
593 infection. Journal of gastrointestinal and liver diseases J Gastrointestin Liver Dis. **16**(1): 65-73.

594 3. **Simmonds P, Bukh J, Combet C, Deléage G, Enomoto N, Feinstone S, Halfon P, Inchauspé**
595 **G, Kuiken C, Maertens G, Mizokami M, Murphy DG, Okamoto H, Pawlotsky JM, Penin F,**
596 **Sablon E, Shin-I T, Stuyver LJ, Thiel HJ, Viazov S, Weiner AJ, Widell A**. 2005. Consensus
597 proposals for a unified system of nomenclature of hepatitis C virus genotypes. Hepatology **42(4):**
598 962-973.

599 4. **Smith DB, Bukh J, Kuiken C, Muerhoff AS, Rice CM, Stapleton JT, Simmonds P.** 2014.
600 Expanded classification of hepatitis C virus into 7 genotypes and 67 subtypes: updated criteria and
601 genotype assignment web resource. Hepatology. **59(1):** 318-27.

602 5. **Belousova V, Abd-Rabou AA, Mousa SA.** 2015. Recent advances and future directions in the
603 management of hepatitis C infections. Pharmacology & therapeutics **145C**: 92-102.

604 6. **Lawitz E, Sulkowski MS, Ghalib R, Rodriguez-Torres M., Younossi ZY, Corregidor A,**
605 **Edwin DeJesus, Brian Pearlman, Mordechai Rabinovitz, Norman Gitlin, Joseph K Lim,**
606 **Pockros PJ, Scott JD, Fevery B, Lambrecht T, Ouwerkerk-Mahadevan S, Callewaert K,**
607 **Symonds WT, Picchio G, Lindsay KL, Beumont M, Jacobson IM**. 2014. Simeprevir plus
608 sofosbuvir, with or without ribavirin, to treat chronic infection with hepatitis C virus genotype 1 in
609 non-responders to pegylated interferon and ribavirin and treatment-naive patients: the COSMOS
610 randomised study. The Lancet **384**(9956), 1756–1765.

Journal of Virology

7. **Koretz, RL.** 2014. Review: Telaprevir, boceprevir, simeprevir, or sofosbuvir improves response in HCV type 1. Annals of Internal Medicine **161**(10): JC11.
8. **Brett D. Lindenbach & Charles M. Rice,** 2013. The ins and outs of hepatitis C virus entry and assembly. Nature Reviews Microbiology **11**(10):688-700.
9. **Goffard A & Dubuisson J**, 2003. Glycosylation of hepatitis C virus envelope proteins. Biochimie **85**(3-4):295-301.
10. **Pileri P, Uematsu Y, Campagnoli S, Galli G, Falugi F, Petracca R, Weiner AJ, Houghton M, Rosa D, Grandi G, Abrignani S.** 1998. Binding of hepatitis C virus to CD81. Science **282**(5390): 938-941.
11. **Scarselli E, Ansuini H, Cerino R, Roccasecca RM, Acali S, Filocamo G, Traboni C, Nicosia A, Cortese R, Vitelli A.** 2002. The human scavenger receptor class B type I is a novel candidate receptor for the hepatitis C virus. The EMBO Journal **21**(19): 5017-5025.
12. **Owsianka AM, Timms JM, Tarr AW, Brown RJ, Hickling TP, Szwejk A, Bienkowska-Szewczyk K, Thomson BJ, Patel AH, Ball JK.** 2006. Identification of conserved residues in the E2 envelope glycoprotein of the hepatitis C virus that are critical for CD81 binding. Journal of Virology **80**(17): 8695-8704.
13. **Drummer HE, Boo I, Maerz AL, Poumbourios P.** 2006. A conserved Gly436-Trp-Leu-Ala-Gly-Leu-Phe-Tyr motif in hepatitis C virus glycoprotein E2 is a determinant of CD81 binding and viral entry. Journal of Virology **80**(16):7844-53.
14. **Owsianka A, Tarr AW, Juttla VS, Lavillette D, Bartosch B, Cosset FL, Ball JK, Patel AH.** 2005. Monoclonal antibody AP33 defines a broadly neutralizing epitope on the hepatitis C virus E2 envelope glycoprotein. Journal of Virology **79**(17): 11095-11104.

15. **Flint M, Maidens CM, Loomis-Price LD, Shotton C, Dubuisson J, Monk, P, Higginbottom A, Levy S and McKeating JA**. 1999. Characterization of hepatitis C virus E2 glycoprotein interaction with a putative cellular receptor, CD81. Journal of Virology **73**(8): 6235-6244.

16. **Broering TJ, Garrity KA, Boatright NK, Sloan SE, Sandor F, Thomas WD Jr, Szabo G, Finberg RW, Ambrosino DM, Babcock GJ**. 2009. Identification and characterization of broadly neutralizing human monoclonal antibodies directed against the E2 envelope glycoprotein of hepatitis C virus. Journal of Virology **83**(23): 12473-12482.

17. **Keck Z, Wang W, Wang Y, Lau P, Carlsen TH, Prentoe J, Xia J, Patel AH, Bukh J, Foung SK**. 2013. Cooperativity in virus neutralization by human monoclonal antibodies to two adjacent regions located at the amino terminus of hepatitis C virus E2 glycoprotein. Journal of Virology **87**(1): 37-51.

18. **Pantua H, Diao J, Ultsch M, Hazen M, Mathieu M, McCutcheon K, Takeda K, Date S, Cheung TK, Phung Q, Hass P, Arnott D, Hongo JA, Matthews DJ, Brown A, Patel AH, Kelley RF, Eigenbrot C, Kapadia SB.** 2013. Glycan shifting on hepatitis C virus (HCV) E2 glycoprotein is a mechanism for escape from broadly neutralizing antibodies. Journal of Molecular Biology **425**(11): 1899-1914

19. **Kong L, Jackson KN, Wilson I and Law M.** 2015. Capitalizing on knowledge of hepatitis C virus neutralizing epitopes for rational vaccine design. Current Opinion in Virology **11**:148–157.

20. **Zhang P, Zhong L, Struble EB, Watanabe H, Kachko A, Mihalik K, Virata-Theimer ML, Alter HJ, Feinstone S, Major M.** 2009. Depletion of interfering antibodies in chronic hepatitis C patients and vaccinated chimpanzees reveals broad cross-genotype neutralizing activity. Proceedings of the National Academy of Sciences of the United States of America **106**(18): 7537-7541.

21. **Keck ZY, Xia J, Wang Y, Wang W, Krey T, Prentoe J, Carlsen T, Li AY, Patel AH, Lemon SM, Bukh J, Rey FA, Foung SK.** 2012. Human monoclonal antibodies to a novel cluster of conformational epitopes on HCV E2 with resistance to neutralization escape in a genotype 2a isolate. PLoS Pathog. **8**(4):e1002653. doi: 10.1371/journal.ppat.1002653.

22. **Johansson DX, Voisset C, Tarr AW, Aung M, Ball JK, Dubuisson J, Persson MA.** 2007. Human combinatorial libraries yield rare antibodies that broadly neutralize hepatitis C virus. Proceedings of the National Academy of Sciences of the United States of America **104**(41): 16269-16274.

23. **Keck ZY, Li TK, Xia J, Gal-Tanamy M, Olson O, Li SH, Patel AH, Ball JK, Lemon SM, Foung SK.** 2008. Definition of a conserved immunodominant domain on hepatitis C virus E2 glycoprotein by neutralizing human monoclonal antibodies. Journal of Virology **82**(12): 6061-6066.

24. **Law M, Maruyama T, Lewis J, Giang E, Tarr AW, Stamataki Z, Gastaminza P, Chisari FV, Jones IM, Fox RI, Ball JK, McKeating JA, Kneteman NM, Burton DR**. 2008. Broadly neutralizing antibodies protect against hepatitis C virus quasispecies challenge. Nature Medicine **14**(1): 25-27.

25. **Ball JK, Tarr AW, McKeating JA.** 2014. The past, present and future of neutralizing antibodies for hepatitis C virus. Antiviral Res. **105**: 100-11.

26. **Potter JA, Owsianka AM, Jeffery N, Matthews DJ, Keck ZY, Lau P, Foung SK, Taylor GL, Patel AH.** 2012. Toward a hepatitis C virus vaccine: the structural basis of hepatitis C virus neutralization by AP33, a broadly neutralizing antibody. Journal of Virology **86**(23): 12923-12932.

27. **Kong L, Giang E, Nieusma T, Robbins JB, Deller MC, Stanfield RL, Wilson IA, Law M.** 2012. Structure of hepatitis C virus envelope glycoprotein E2 antigenic site 412 to 423 in complex with antibody AP33. Journal of Virology **86**(23): 13085-13088.

28. **Kong L, Giang E, Robbins JB, Stanfield RL, Burton DR, Wilson IA, Law M.** 2012. Structural basis of hepatitis C virus neutralization by broadly neutralizing antibody HCV1. Proceedings of the National Academy of Sciences of the United States of America **109**(24): 9499-9504.

29. **Khan AG, Whidby J, Miller MT, Scarborough H, Zatorski AV, Cygan A, Price AA, Yost SA, Bohannon CD, Jacob J, Grakoui A, Marcotrigiano J.** 2014. Structure of the core ectodomain of the hepatitis C virus envelope glycoprotein 2. Nature **509**(7500): 381-384.

30. **Kong L, Giang E, Nieusma T, Kadam RU, Cogburn KE, Hua Y, Dai X, Stanfield RL, Burton DR, Ward AB, Wilson IA, Law M.** 2013. Hepatitis C virus E2 envelope glycoprotein core structure. Science **342**(6162): 1090-1094

31. **Tarr AW, Owsianka AM, Timms JM, McClure CP, Brown RJ, Hickling TP, Pietschmann T, Bartenschlager R, Patel AH, Ball JK.** 2006. Characterization of the hepatitis C virus E2 epitope defined by the broadly neutralizing monoclonal antibody AP33. Hepatology. **43**(3): 592-601.

32. **Clayton RF, Owsianka A, Aitken J, Graham S, Bhella D, Patel AH.** 2002. Analysis of antigenicity and topology of E2 glycoprotein present on recombinant hepatitis C virus-like particles. Journal of Virology **76**(15): 7672-7682.

33. **Fields GB, Noble RL** 1990. Solid phase peptide synthesis utilizing 9 fluorenylmethoxycarbonyl amino acids. Int. J. Pept. Protein Res. 35(3): 161-214.

34. **Verdoliva A, Marasco D, De Capua A, Saporito A, Bellofiore P, Manfredi V, Fattorusso R, Pedone C, Ruvo M**. 2005. A new ligand for immunoglobulin g subdomains by screening of a synthetic peptide library. Chembiochem. **6**(7): 1242-1253.

35. **Saporito A, Marasco D, Chambery A, Botti P, Monti SM, Pedone C, Ruvo M.** 2006. The chemical synthesis of the GstI protein by NCL on a X-Met site. Biopolymers. **83**(5): 508-18.

36. **Carter JM**. Techniques for conjugation of synthetic peptides to carrier molecules. 1994. Methods Mol. Biol. **36**: 155-91.

37. **Kohler G, Milstein C.** 1976. Derivation of specific antibody-producing tissue culture and tumor lines by cell fusion. European Journal of Immunology **6**(7): 511-519.

38. **Focà A, Sanguigno L, Focà G, Strizzi L, Iannitti R, Palumbo R, Hendrix MJC, Leonardi A, Ruvo M, Sandomenico A.** 2015. New Anti-Nodal Monoclonal Antibodies Targeting the Nodal Pre-Helix Loop Involved in Cripto-1 Binding. Int. J. Mol. Sci. **16**(9), 21342-21362.

39. **Patel AH, Wood J, Penin F, Dubuisson J, McKeating JA.** 2000. Construction and characterization of chimeric hepatitis C virus E2 glycoproteins: analysis of regions critical for glycoprotein aggregation and CD81 binding. J Gen Virol **81**(12): 2873-2883.

40. **Wakita T, Pietschmann T, Kato T, Date T, Miyamoto M, Zhao Z, Murthy K, Habermann A, Kräusslich HG, Mizokami M, Bartenschlager R, T Liang J.** 2005. Production of infectious hepatitis C virus in tissue culture from a cloned viral genome. Nat Med. **11**(7): 791–796.

41. **Keck Z-y, Angus AGN, Wang W, Lau L, Wang Y, Gatherer D, Patel A, Foung SKH.** 2014. Non-random Escape Pathways from a Broadly Neutralizing Human Monoclonal Antibody Map to a Highly Conserved Region on the Hepatitis C Virus E2 Glycoprotein Encompassing Amino Acids 412–423. PLoS Pathog **10**(8): e1004297.

42. **Iro M, Witteveldt J, Angus AG, Woerz I, Kaul A, Bartenschlager R, Patel AH.** 2009. A reporter cell line for rapid and sensitive evaluation of hepatitis C virus infectivity and replication. Antiviral research **83**(2): 148-155.

43. **Jankarik J, Kim S.** 1991. Sparse matrix sampling: a screening method for crystallization of proteins. J Appl Crystallogr **24**: 409-411.

44. **Otwinowski Z, Minor W.** 1997. Processing of X-ray Diffraction Data Collected in Oscillation Mode. Methods in Enzymology **276**: 307-326.

45. **McCoy AJ, Grosse-Kunstleve RW, Adams PD, Winn MD, Storoni LC, Read RJ.** 2007. Phaser crystallographic software. Journal of applied crystallography **40**: 658-674.

46. **Morris RJ, Perrakis A, Lamzin VS.** 2002. ARP/wARP's model-building algorithms. I. The main chain. Acta crystallographica. Section D, Biological crystallography **58**: 968-975.

47. **Winn MD, Murshudov GN, Papiz MZ**. 2003. Macromolecular TLS refinement in REFMAC at moderate resolutions. Methods in Enzymology **374**: 300-321

48. **Emsley P, Cowtan K.** 2004. Coot: model-building tools for molecular graphics. Acta crystallographica. Section D, Biological crystallography **60**: 2126-2132.

49. **Van Der Spoel D, Lindahl E, Hess B, Groenhof G, Mark AE, Berendsen HJ**. 2005. GROMACS: fast, flexible, and free. J Comput Chem. **26**(16):1701-18.

50. **Stanfield RL, Zemla A, Wilson IA, Rupp B.** 2006. Antibody elbow angles are influenced by their light chain class. Journal of Molecular Biology **357**(5): 1566-1574.

51. **Chothia C, Lesk AM, Tramontano A, Levitt M, Smith-Gill SJ, Air G, Sheriff S, Padlan EA, Davies D, Tulip WR, et al.** 1989. Conformations of immunoglobulin hypervariable regions. Nature **342**(6252): 877-883

52. **Shen Y, Maupetit J, Derreumaux P, Tufféry P.** 2014. Improved PEP-FOLD approach for peptide and miniprotein structure prediction J. Chem. Theor. Comput. **10**: 4745-4758.

53. **Li Y, Pierce BG, Wang Q, Keck ZY, Fuerst TR, Foung SK, Mariuzza RA**. 2015. Structural basis for penetration of the glycan shield of hepatitis C virus E2 glycoprotein by a broadly neutralizing human antibody. J Biol Chem. **290**(16):10117-25.

54. **Meola A, Tarr AW, England P, Meredith LW, McClure CP, Foung SK, McKeating JA, Ball JK, Rey FA, Krey T.** 2015. Structural Flexibility of a Conserved Broadly Neutralizing Epitope in Hepatitis C Virus Glycoprotein E2. Journal of Virology **89**(4): 2170-81.

766 **Figure legends**

767 **Figure 1.** Selection of MAbs specifically binding to the cyclic variant of epitope I. **(A)** Primary structure
768 of C-Epitope I peptide representing the HCV E2 region from residues 412 to 422. The peptide was C-
769 terminally amidated and N-terminally acetylated and cyclized using two cysteines introduced at either end
770 of the native sequence (underlined). **(B)** ELISA screening of hybridoma supernatants. C-Epitope I and L-
771 Epitope I were coated onto microtitre plates at 0.5 µg/ml. Hybridoma supernatants were added and bound
772 antibodies detected with an HRP-conjugated anti-mouse antibody. Trastuzumab was used at the same
773 concentration as a negative control (NC). (**C**) Dose-dependent binding of purified MAbs C1-C7 to C-
774 Epitope I. The MAbs did not bind to L-Epitope I or BSA_2 (glutaraldehyde-self conjugated BSA); only the
775 negative binding data for MAb C2 are shown. (D) Binding of MAb AP33 to L- and C-Epitope I peptide.

776

777 **Figure 2A-L:** Overlay of sensorgrams showing the binding of C-Epitope I at concentrations ranging
778 between 6.5 nM and 10 µM to MAbs C1 (**A**), C2 (**B**), C3 (**C**), C4 (**D**), C5 (**E**), C6 (**F**), C7 (**G**)
779 immobilized on Biacore CM5 sensorchips. **H**: Overlay of sensorgrams obtained following the injection of
780 L-Epitope I at the highest concentration of 10 µM, onto the 7 MAbs immobilized on Biacore CM5 sensor
781 chips. Overlay of sensorgrams showing the binding of C-Epitope I (**I**) and L-Epitope I (**L**) to MAb AP33
782 immobilized on Biacore CM5 sensorchips. Dose response assays were carried out at the indicated
783 concentrations. All experiments were carried out at 25 °C, at a constant flow rate of 20 µl/min using HBS
784 as running buffer. Binding parameters are reported in Table 1.

785

786 **Figure 3A-H:** Overlay of sensorgrams showing the dose-dependent binding of MAbs C2, C3, C4, C6, C7
787 (**A-E**) and AP33 (**F**) to soluble E2 (sE2) recombinant protein immobilized on Biacore sensor chips. No
788 interaction was detected using an IgG1 isotype at the concentrations of 5 µM (**G**). All experiments were
789 carried out at 25 °C, at a constant flow rate of 20 µl/min using HBS as running buffer. Binding

parameters are reported in Table 2. **H**: SDS-PAGE analysis (12% bis-acrylamide) of purified sE2 used for SPR binding studies. Lane M: protein standards Precision Plus Protein Standards (10-250 kDa, Biorad). Lane 1: 2 µg of purified sE2 under reducing conditions respectively. Proteins were visualized by Bio-Safe Coomassie Blue stain.

Figure 4. Binding of MAbs to envelope glycoproteins in ELISA. ~~Purified sE2 at 5 µg/ml and 0.5 µg/ml~~ and HEK cell lysates containing sE2, FL E2 and E1E2 were incubated on GNA-coated wells, followed by addition of MAb AP33 (0.02 µg/ml) or C2-C5 and C7 (10 µg/ml). The bound antibodies were detected using HRP-conjugated anti-mouse IgG.

Figure 5. Neutralization of WT and N417T mutant HCVcc by MAbs AP33 and C2. (**A**) Wild type (WT) JFH1 HCVcc or (**B**) HCVcc carrying the N417T mutation were incubated with a range of concentrations of MAb AP33 or C2 prior to infection of Huh7-J20 cells. At 72 h post-infection, the reporter SEAP activity secreted into the cell medium was measured and the infectivity levels plotted as % infectivity relative to 'no antibody' control.

Figure 6. Structure of Fab C2 in complex with the C-epitope I peptide (**A**) Overview of the C-Epitope I peptide bound in the Fab C2 combining site. The peptide carbon atoms are ramp-colored from the N-terminus (blue) to the C-terminus (red) through green. (**B**) 2Fo-Fc electron density map of the peptide region contoured at 1.0 σ. (**C**) Backbone intrapeptide H-bonds. (**D**) H-bond and (**E**) hydrophobic interactions at the peptide-Fab C2 interface.

Figure 7. Intrinsic conformational properties of the cyclic peptide. (**A**) RMSD values computed on the Cα atoms of the MD trajectory frames against the starting structure. (**B**) Time evolution of the radius of gyration computed on the Cα atoms of the peptide. (**C**) Far-UV CD spectrum of the peptide in phosphate buffer at neutral pH. (**D**) RMSD values computed on the Cα atoms of the trajectory frames against the conformation of the liner peptide in the complex with AP33 (gray line, PDB code 4GAG). RMSD values of the trajectory structures versus the starting conformation of the cyclic peptide (black) are shown for comparative purposes.

Figure 8. Comparison of conformations adopted by epitope 412-422 peptides in complex with Fabs. (**A**) Structural alignment of peptides bound to AP33 (blue) and to Fab C2 (magenta) shows similar β-hairpin conformations. (**B**) The crystal structures of Fab C2 (orange, this study) and AP33 Fab (purple, pdb code 4GAG) are superimposed and faded out. The peptide carbon atoms are ramp-colored from the N-terminus (blue) to the C-terminus (red) through green, to show that the two peptides are bound in opposite orientations relative to the Fab. (**C**) Superimposition of the cyclic peptide (with the carbon atoms in orange) to the linear peptide in its complex with AP33. (**D**) The peptide structures in the complexes with Fab C2 (orange) and AP33 Fab (purple) are aligned to show how the two antibodies approach the opposite surfaces of the peptide hairpin-like structure.

Figure 9. Histogram showing the buried area for the 412-412 residues in different peptide Fab complex. 4GAG and 4G6A correspond to two independent characterizations of the complex between AP33 and the linear epitope (26, 27). 4DGV is the complex between HCV1 and the linear peptide (28); 5EOC is the structure described in this work (Fab C2).

Journal of Virology

TABLE 1. Affinity of antibodies to cyclic and linear epitope 412-422. Association and dissociation rates and dissociation constants were obtained by SPR for the binding of C-Epitope I and L-Epitope to MAbs C1 to C7 and AP33. Data were analyzed using the BiaEvaluation 4.2 software.

	C-Epitope I			L-Epitope I		
MAb	K_a(1/Ms)	K_d(1/s)	K_D (M)	K_a(1/Ms)	K_d(1/s)	K_D (M)
C1	$4.84*10^5$	$1.20*10^{-2}$	$2.48*10^{-8}$	-	-	N.B.
C2	$4.07*10^5$	$1.23*10^{-2}$	$3.03*10^{-8}$	-	-	N.B.
C3	$3.21*10^5$	$1.01*10^{-2}$	$3.14*10^{-8}$	-	-	N.B.
C4	$2.82*10^5$	$1.25*10^{-2}$	$4.42*10^{-8}$	-	-	N.B.
C5	$4.34*10^5$	$5.52*10^{-3}$	$1.27*10^{-8}$	-	-	N.B.
C6	$3.59*10^5$	$3.22*10^{-4}$	$8.97*10^{-10}$	-	-	N.B.
C7	$3.56*10^5$	$2.44*10^{-4}$	$6.86*10^{-10}$	-	-	N.B.
AP33	$1.21*10^4$	$8.62*10^{-4}$	$7.11*10^{-8}$	$9.99*10^5$	$5.34*10^{-4}$	$5.35*10^{-10}$

N.B.: No Binding

TABLE 2. Affinity of antibodies to sE2. Association and dissociation rates and dissociation constants were obtained by SPR for the binding of MAbs C2, C3, C4, C5, C7, AP33 and un-related mouse IgG1 to sE2. The binding of C2 and AP33 Fabs to immobilized sE2 was measured to assess avidity effects exhibited by the full antibodies. Data were analyzed using the BiaEvaluation 4.2 software

MAb or fragment	K_a(1/Ms)	K_d(1/s)	K_D (M)
C2	$1.88*10^4$	$8.48*10^{-4}$	$49.8*10^{-9}$
C3	$3.24*10^4$	$7.35*10^{-4}$	$41.6*10^{-9}$
C4	$1.54*10^4$	$5.38*10^{-4}$	$44.6*10^{-9}$
C5	$2.23*10^4$	$7.31*10^{-4}$	$46.8*10^{-9}$
C7	$3.08*10^3$	$2.57*10^{-4}$	$83.4*10^{-9}$
AP33	$6.49*10^5$	$6.40*10^{-5}$	$0.142*10^{-9}$
Fab C2	$1.28*10^4$	$4.63*10^{-3}$	$301*10^{-9}$
Fab AP33	$2.30*10^5$	$1.47*10^{-4}$	$0.72*10^{-9}$
IgG1 isotype control	-	-	N.B.

N.B.: No Binding

924 **TABLE 3.** Data collection and refinement statistics. Values in parenthesis refer to the 2.05-1.98 Å
925 resolution shell.
926

Data collection statistics	
Space group	P1
Cell parameters	
a(Å), b(Å), c(Å), α(°), β(°), γ(°)	54.97, 56.19, 77.15, 90.34, 90.18, 94.98
Resolution range(Å)	25.0-1.98
Number of molecule in the asymmetric unit	2
Number of unique observations	59746
Multiplicity	2.9 (1.9)
Completeness (%)	93.0 (81.7)
R_{merge}[a]	0.077 (0.476)
I/σ(I)	15.9 (1.7)
Refinement statistics	
Resolution range (Å)	15.0-19.8
R_{factor}[b]/R_{free}[c]	0.224/0.267
Number of protein/peptide atoms	13092
Number of water molecules	510
Root mean square deviations from ideality	
Bonds (Å)	0.0020
Angles (°)	1.30

[a] $R_{merge} = \Sigma_{hkl}\Sigma_i|I_i(hkl) - \langle I(hkl)\rangle|/\Sigma_{hkl}\Sigma_i I_i(hkl)$, where $I_i(hkl)$ is the intensity of an observation and $\langle I(hkl)\rangle$ is the mean value for its unique reflection; summations are over all reflections.

[b] $R_{factor} = \Sigma_h|Fo(h) - Fc(h)|/\Sigma_h Fo(h)$, where Fo and Fc are the observed and calculated structure-factor amplitudes, respectively.

[c] R_{free} was calculated with 5% of the data excluded from the refinement.

927
928

929 **TABLE 4**. Binding affinity of Fab C2 to the epitope I variants used in this study. Association and
930 dissociation rates and K_D values were determined by SPR for the binding of peptides to Fab C2. Data
931 were derived using BiaEvaluation software ver. 4.2.

932

Peptide	Sequence[†]	K_D (M)	K_a (1/s)	K_d (1/Ms)
C-Epitope I	KKCQLINTNGSWHIC	$3.27*10^{-8}$	$4.77*10^{5}$	$1.56*10^{-2}$
L-Epitope I	KKC(methyl)QLINTNGSWHIC(methyl)	N.B.	0	0
C-Epitope I Mut I	KKCAAANTNGSWHIC	$4.53*10^{-7}$	$1.22*10^{6}$	$5.53*10^{-1}$
C-Epitope I Mut II	KKCQLIAAAGSWHIC	$1.48*10^{-8}$	$3.2*10^{3}$	$4.73*10^{-5}$
C-Epitope I Mut III	KKCQLINTNEEWHIC	$4.67*10^{-6}$	$1.62*10^{4}$	$7.54*10^{-2}$
C-Epitope I Mut IV	KKCQLINTNGSAAAC	N.B.	0	0

933

934 [†] In C-Epitope I and related mutants I-IV, a disulphide bridge connects the two cysteines. In L-Epitope I, cysteines
935 are methylated. Methylation is the minimum molecular modification to block reactive thiols. Mutated peptides I, II
936 and IV were designed and prepared to replace native residues with alanines. In mutant III, glycine and serine were
937 mutated to glutamic acid because alanines are too similar to glycine and serine. N.B.: No Binding

938

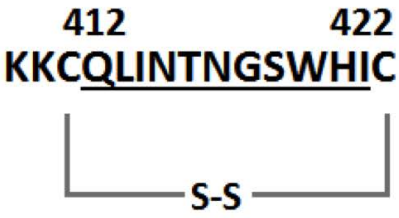

A

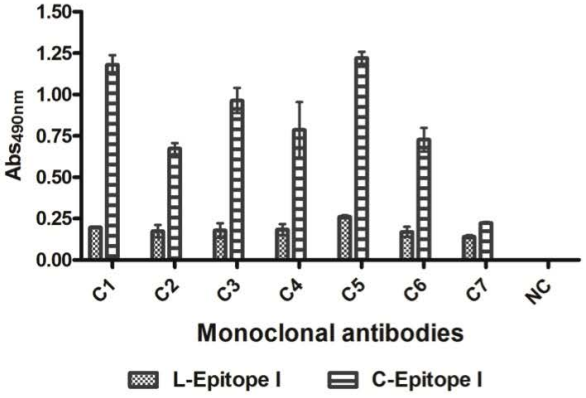

B

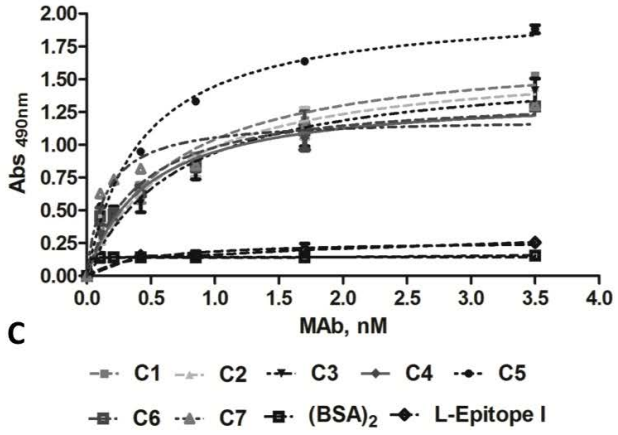

C

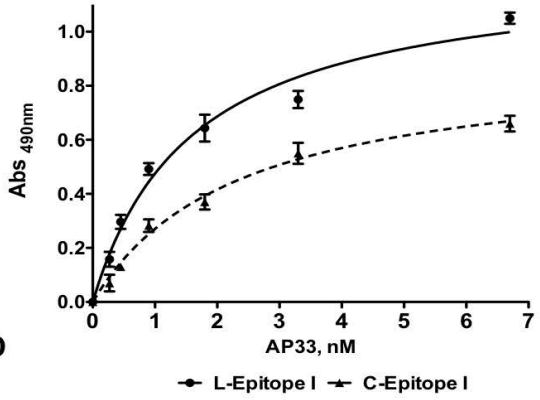

D

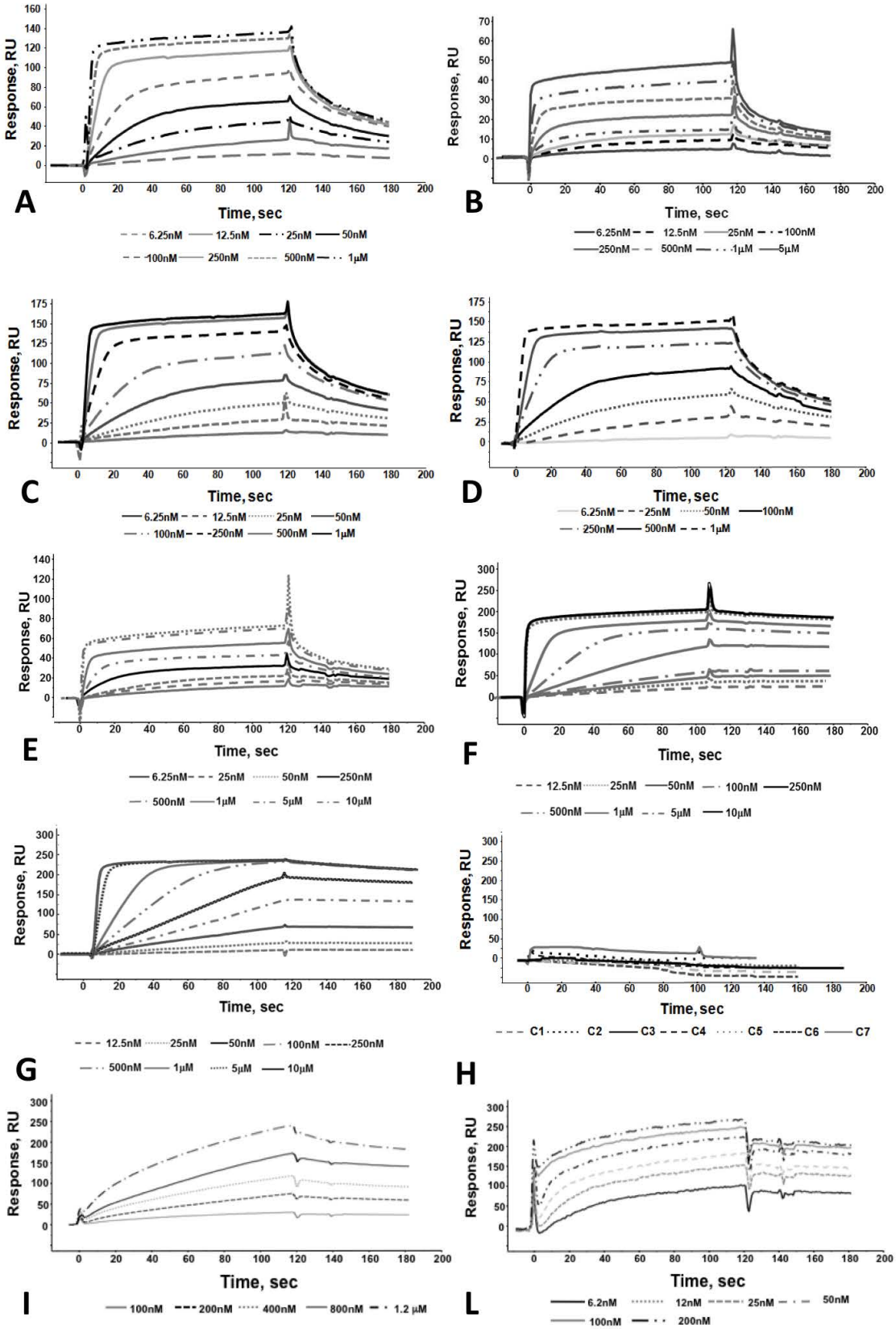

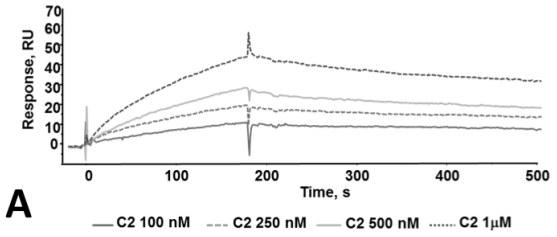

A

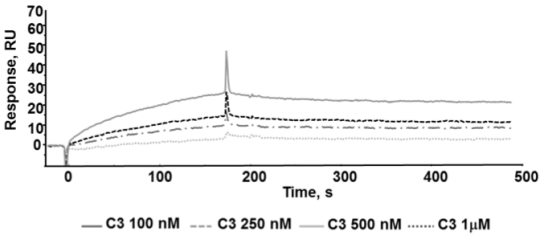

B

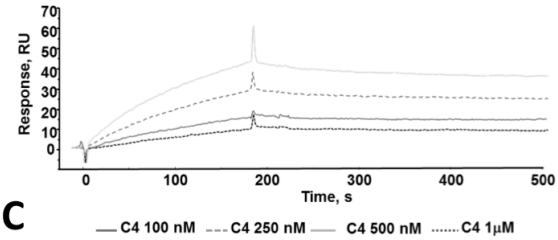

C

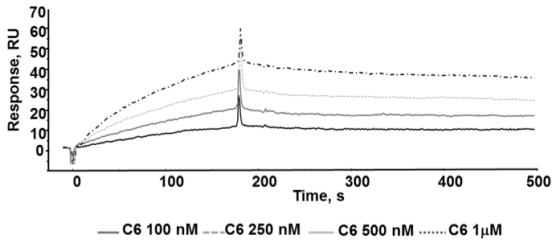

D

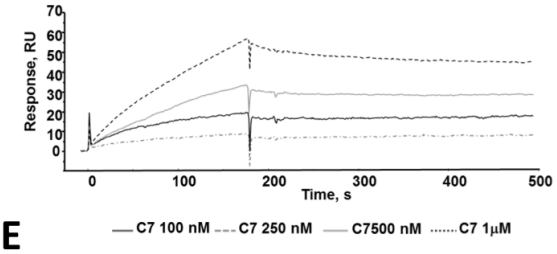

E

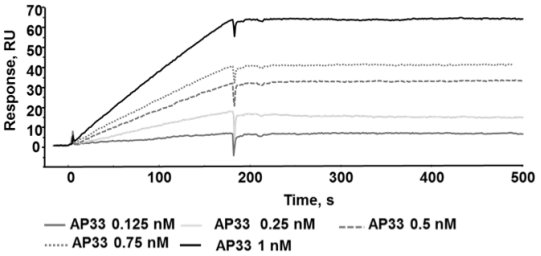

F

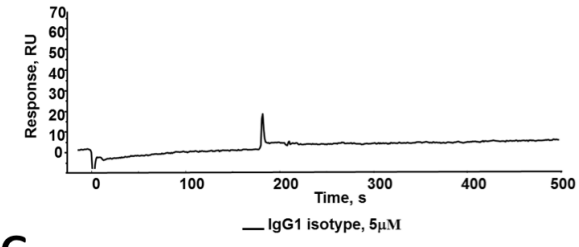

G

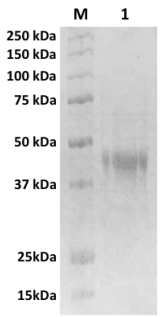

H

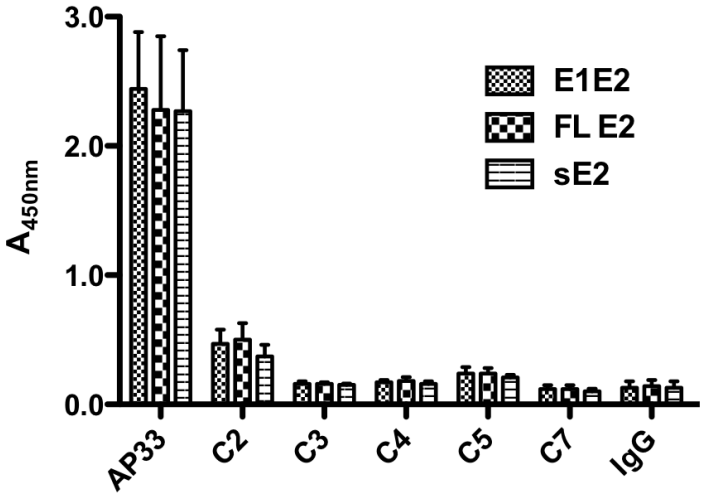

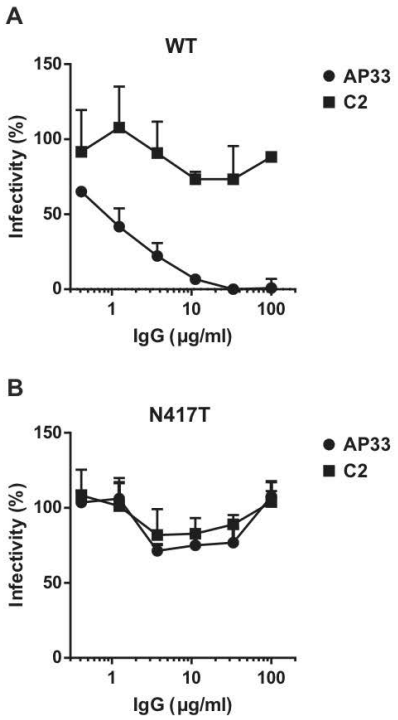

A

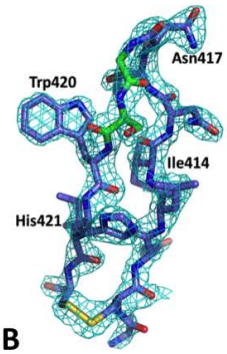

B

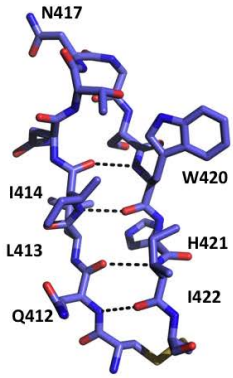

C

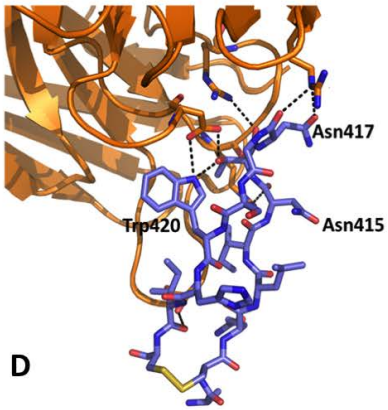

D

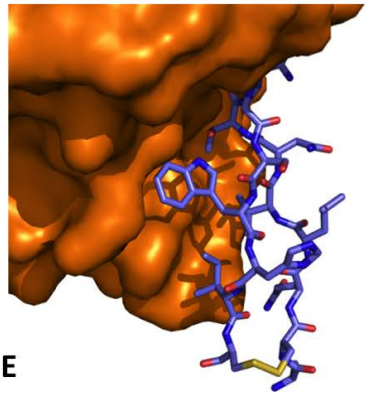

E

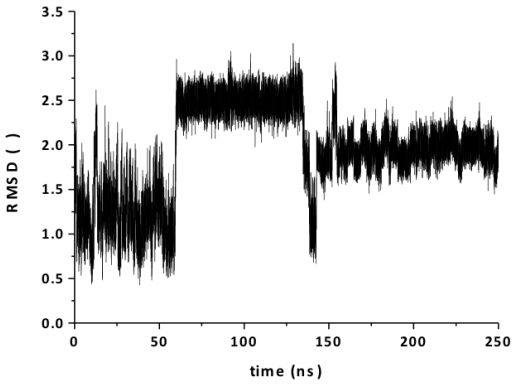

A

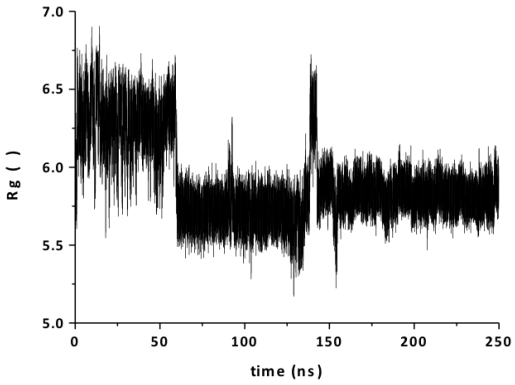

B

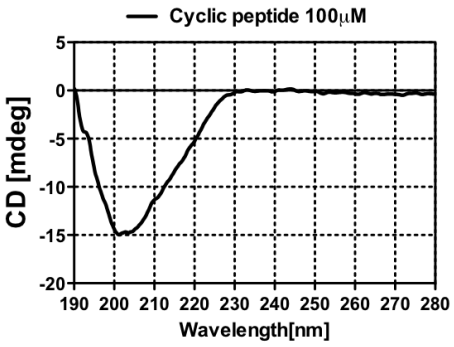

C

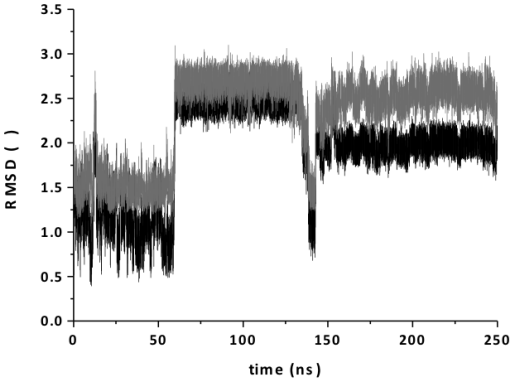

D